The Effect of System Pressure on Gas-Liquid Slug Flow in a Microchannel

Chaoqun Yao and Zhengya Dong
Dalian National Laboratory for Clean Energy, Dalian Institute of Chemical Physics, Chinese Academy of Sciences, Dalian 116023, China

University of Chinese Academy of Sciences, Beijing 100049, China

Yuchao Zhao and Guangwen Chen
Dalian National Laboratory for Clean Energy, Dalian Institute of Chemical Physics, Chinese Academy of Sciences, Dalian 116023, China

DOI 10.1002/aic.14306
Published online December 11, 2013 in Wiley Online Library (wileyonlinelibrary.com)

Characteristics of gas-liquid two-phase flow under elevated pressures up to 3.0 MPa in a microchannel are investigated to provide the guidance for microreactor designs relevant to industrial application. The results indicate that a strong leakage flow through the channel corners occurs although the gas bubbles block the channel. With a simplified estimation, the leakage flow is shown to increase with an increase in pressure, leading to a bubble formation shifting from transition regime to squeezing regime. During the formation process, the two-phase dynamic interaction at the T-junction entrance would have a significant influence on the flow in the main channel as the moving velocity of generated bubbles varies periodically with the formation cycle. Other characteristics such as bubble formation frequency, bubble and slug lengths, bubble velocities, gas hold-up, and the specific surface area are also discussed under different system pressures. © 2013 American Institute of Chemical Engineers *AIChE J*, 60: 1132–1142, 2014
Keywords: microreactor, microfluidic, hydrodynamics, multiphase, high pressure

Introduction

Microreaction technology is an important method for process intensification. Microreactors are characterized by high mass- and heat-transfer rate, which is especially suitable for highly exothermic and fast reactions or mass-transfer limited processes. Other advantages such as the numbering up mode and miniaturization reduce greatly the investment in both time and expenses from lab research to industrial application. Moreover, microreaction technology features enhanced safety because of the low hold-up and limited damage when hazardous situation happens.

Gas-liquid processes are widely involved in chemical industry. Many researches have shown that microreactors have unique advantages for various gas-liquid system,[1,2] such as absorption[3–6] and reaction.[7–9] For the design and operation of gas-liquid microreactors, a great number of studies dedicated to two-phase hydrodynamics[10,11] and mass transfer[6,12,13] in microchannels have been carried out. Slug flow is obtained for a large range of operating conditions and characterized by sequences of a gas bubble and a liquid slug. The gas bubbles are of regular size and surrounded by a thin liquid film with the bubble body occupying almost the entire channel cross section.[14,15] Low axial mass transfer or back mixing occurs between two adjacent liquid slugs. Both radial mass and heat transfer can be intensified by internal circulation in the liquid slug.[16,17] Given these merits, slug flow is an ideal flow pattern for improving the gas-liquid reaction performance. However, the existing studies on slug flow are mostly under atmospheric conditions, which do not represent the conditions in the majority of gas-liquid reactions in the chemical industry. The transport and reaction characteristics of slug flow under elevated pressures are, therefore, very important from an industrial point of view.

It is known that higher pressure increases the concentration of the dissolved gas in the liquid phase, which is beneficial to the reaction. Moreover, the system pressure can have a considerable influence on the flow and mass-transfer behavior in gas-liquid systems due to gas compressibility. Many literatures[18–20] have reported the influence of the system pressure in bubble columns. Letzel et al.[19] studied the gas hold-up and mass transfer in bubble columns at elevated pressures from 0.1 to 1.3 MPa and found that the gas hold-up and the volumetric mass-transfer coefficient both increased with the increasing system pressure. Maalej et al.[20] measured the mass-transfer coefficient and the specific surface area with the Danckwerts plot method. The results showed a positive influence of pressure on the specific surface area whereas no obvious effect on the liquid side mass-transfer coefficient. Recently, more and more attention has been paid to exploiting applications of high-pressure microfluidics.[8,9,21,22] Keybl and Jensen[8] developed a high-pressure

Correspondence concerning this article should be addressed to G. Chen at gwchen@dicp.ac.cn.

gas-liquid system for determining the homogeneous catalyst kinetic parameters with high efficacy and reproducibility. A detailed introduction of design and packaging of microreactors for high-pressure and high-temperature applications was reviewed by Marre et al.[21] While high-pressure microfluidics can be easily obtained with materials such as stainless steel, to build a high pressure system with transparent materials for the study of gas-liquid flow is much more difficult. Trachsel et al.[9] validated slug flow with laser-induced florescence in a transparent silicon/glass microreactor. However, their work mainly focused on the reaction performance and no detailed information about the flow behavior was reported. Zhao et al.[23] studied the gas-liquid flow patterns under different pressures and found that the transition line between bubbly flow and slug flow shifts to a higher gas-phase Weber number (We_{GS}) and a lower liquid-phase Weber number (We_{LS}) when the system pressure is elevated. Besides the limited number of studies in the literature, another observation is that there is still a lack of detailed knowledge about the characteristics of gas-liquid flow and mass transfer under elevated pressures in microchannels, especially for slug flow.

This work aims at improving our fundamental understanding on slug flow under different pressures, which would be a useful guidance for the industrial applications of gas-liquid microreactors. The pressure effect on the gas bubble generation process, the length of gas bubbles and liquid slugs, bubble velocities, gas hold-up, and the specific surface area, will be investigated through flow visualization in a rectangular microchannel with T-junction at its entrance. To meet the high-throughput requirements in the case of practical industrial implementation, the experimental conditions here were chosen at high Re ranging from 120 to 580, whereas at very low Ca ranging from 0.004 to 0.016. Under such conditions, the slug flow behavior is greatly influenced by the inertial effects, which was discussed in detail in our previous work.[24]

Experimental Setup

The microchannel device used in this work was fabricated on a transparent polyaryl sulfone (PASF) substrate by using micromachining technology in our CNC Machining Center (FANUC KPC-30a). As shown in Figure 1, the inlet configuration of the microchannel is a T-shaped junction. All the channels have the same rectangular cross section (600 μm in width, 300 μm in depth). The length of the mixing channel is 60 mm. The machined PASF plate was covered by another smooth PAST plate. Both plates were sandwiched between two stainless steel plates and sealed by screws. The sealed microchannel was tested by gas-tightness experiments under 5 MPa and no leakage occurred.

The experiments were conducted under nitrogen-water flow. The experimental setup was shown in Figure 2. Gas flow was provided from a cylinder and controlled by a series of mass flow controllers with different flow ranges (D07-7B, Beijing Sevenstar Electronics, China) and an accuracy of 0.5% full scale. The pressure of the system was controlled by a back pressure valve after the gas-liquid separator. Under each operating pressure, the actual gas flow rate was calibrated by a soap film flow meter downstream the back pressure valve under atmospheric conditions (the separator was filled with gas). During the experiments, the liquid out of the microchannel was stored in the gas-liquid separator

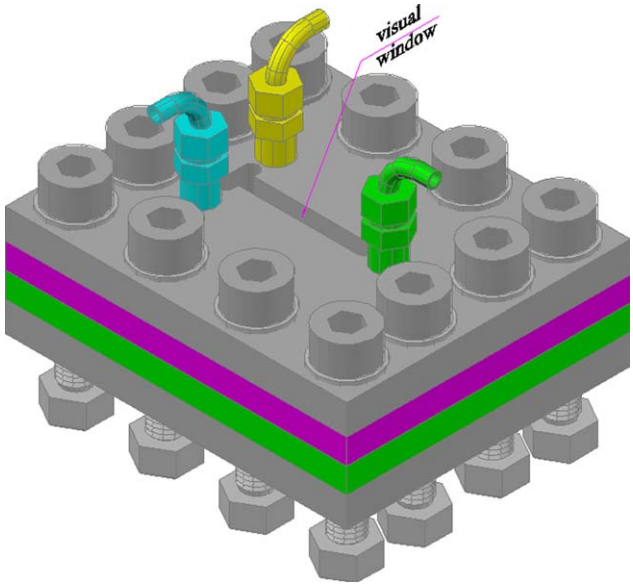

Figure 1. Schematic of the microchannel device.

[Color figure can be viewed in the online issue, which is available at wileyonlinelibrary.com.]

and the outlet gas flow rate after the back pressure valve was also measured by the soap film flow meter. As the liquid occupies space in the separator, the outlet gas flow rate should be equal to the sum of the calibrated gas flow rate (Q_G) and the additional flow rate by liquid ($= Q_L \times P_s/P_a$) where the P_s represents the pressure in the separator. The error between the actual and the calculated outlet flow rate was less than 2%. Deionized water was pumped by a high-precision digital piston pump (Beijing Satellite Manufacturing Factory, measurement range: 0–5 mL/min, precision: 0.3%). The liquid flow rate was also calibrated by weighing method under each run. The buffer tank in the liquid delivering line was to eliminate the pulsation of the flow rate. All the experiments were conducted under room temperature.

The slug flow pattern was recorded by a CMOS high-speed camera system (BASLER A504kc). The CMOS camera was placed above the visual window with a cold light source placed beneath the visual window to provide strong light. In all experiments, the CMOS camera was set to work at a recording rate of 1000 frames/s and a resolution of 1280 $\times$ 512 pixels. The shutter time was set as 80 μs. The shooting zone included the T-junction and the main channel with a length about 13.4 mm downstream the T-junction as shown in Figure 2. Under each operating pressure, four or five experimental conditions were reproduced and the bubble and slug length were compared to examine the reproducibility. We found that the maximum error is 6.8%.

The gas bubbles and liquid slugs in each captured image were extracted by a Matlab program[24] and then parameters such as the gas bubble and liquid slug lengths, bubble velocity, gas hold-up, and the specific surface area were obtained. To calculate the bubble velocity, the moving distance of each bubble was obtained as their centroid location difference from two successive images. Under each operational condition, a sequence of at least 200 images, which corresponded to 300–2000 bubbles, was analyzed and the data were averaged to obtain the final value. The relative standard deviation in the bubble and slug lengths did not exceed 5%.

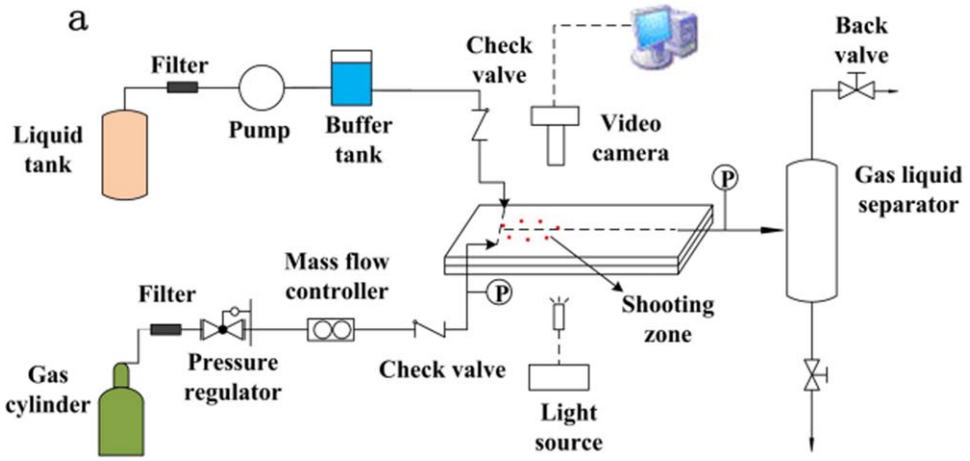

Figure 2. Schematic of the experimental setup.

[Color figure can be viewed in the online issue, which is available at wileyonlinelibrary.com.]

Results and Discussion

Physical properties of fluids and definition of parameters

The system pressure was varied in the range of 0.1–3.0 MPa in the experiments. The solubility of nitrogen in water is only about 0.413 ml (scc)/g at 20°C and 3.0 MPa and, therefore, dissolution of nitrogen can be neglected.[25] Under experimental conditions, the largest pressure drop through the entire microchannel device was about 24 KPa at 3.0 MPa, which only accounts 0.8% of the system pressure, so it is reasonable to assume that the superficial gas velocity (j_G) was kept constant in the microchannel. Thus, j_G was calculated based on the calibrated flow rate at ambient conditions as

$$j_G = \frac{Q_G}{A_{mc}} \cdot \frac{2P_a}{(P_{in} + P_{out})} \tag{1}$$

The superficial liquid velocity was calculated as

$$j_L = \frac{Q_L}{A_{mc}} \tag{2}$$

Bubble formation regime

The gas bubble formation process in microchannels has been widely studied.[26–29] Due to the competition of forces involved in this process, including the interfacial tension, shear stress, and the resistance force or pressure drop, the formation regime could be generally clarified into squeezing regime[26,27] at very low Ca (<0.01) and shearing regime[28,29] when Ca is higher. In the squeezing regime, the forming gas bubble blocks almost the entire microchannel cross section and the rupture of the bubble neck was mainly driven by the pressure buildup across the bubble as discussed by Garstecki et al.[26] If the inertial effect can be neglected, the size of the gas bubble is determined solely by the ratio between the volumetric flow rates of the two immiscible phases for a fixed inlet geometry. While in the shearing regime[28,29] with gas bubbles partly blocking the microchannel, the shear stress and the inertia play an important role in the pinch-off of the bubble neck. Then, the fluid properties would have an pronounced influence on the bubble lengths. In this work, the effect of the system pressure on the gas bubble formation processes are investigated.

Figure 3 shows the gas bubble pinch-off snapshots under different system pressures. The break-up point moves backward to the T-junction as the pressure increases. The transition of the bubble pinch-off regime implies a complex change in multiphase flow behavior at the T-junction as the pressure increases. The pinch-off process under 0.1 and 1.0 MPa is in the transition regime as Ca is close to 0.01 (being 0.0079 and 0.0099 in Figure 3), which is generally considered as the critical value between the squeezing regime and the shearing regime.[26,28,30] The formation process under transition regime is somehow similar to the shearing regime in which the breakup point is located downstream the T-junction. It indicates that the shear stress exerted on the bubble neck plays an important role although the pressure buildup due to the blockage of the microchannel still dominates over the shear stress. When the system pressure is 2.0 or 3.0 MPa, the gas bubble neck ruptures right at the T-jucntion, representing a typical characteristic of squeezing regime. Therefore, the influence of shear stress is less significant than that at low system pressures, which may originate from the increased leakage flow at increased sytem pressures. In rectangular microchannels, the four corners of the channel can never be completely blocked by the gas bubbles due to the surface tension, thus the liquid leaks through them and around the bubbles,[31–33] as shown in Figure 4a.

To evaluate the leakage flow under different pressures, the liquid volume upstream of the forming bubble (V_{liquid} in Figure 4a) in the T-junction was estimated from the two-dimensional (2-D) top-view images by assuming the gas-liquid interface in depth-wise direction was fixed. Due to the interface movement, V_{liquid} increases with time, so fitting V_{liquid} with time and calculating dV_{liquid}/dt allows the estimation of the leakage flow

$$Q_L = \frac{dV_{liquid}}{dt} + Q_{leak} \tag{3}$$

This estimation was achieved by excluding the images in which the bubble neck starts to shrink drastically. The resluts are depicted in Figure 4b. As can be seen, the estimated liquid flow rate at 0.1 MPa is only approximately 80% of the input flow rate, which means that 20% leakage flow occurs. This value is close to the estimation of van Steijn et al.,[32,33] who found that at least 15% of liquid leaks past the bubbles. In a mathematical approach described by Wong et al.,[31] the

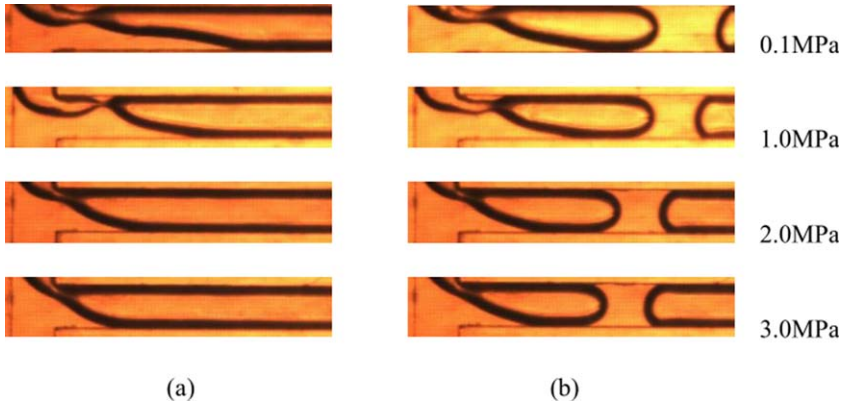

Figure 3. The effect of the system pressure on the bubble formation process (a) $j_G = 0.48$ m/s, $j_L = 0.094$ m/s, $Ca = 0.0079$ and (b) $j_G = 0.48$ m/s, $j_L = 0.23$ m/s, $Ca = 0.0099$.

[Color figure can be viewed in the online issue, which is available at wileyonlinelibrary.com.]

leakage flow scales as $Ca^{-1/3}$ and could be comparable to the bubble velocity under certain conditions. Figure 4b clearly shows that the leakage flow increases with an increase in the system pressure, which may be explained by an increased impingement between the liquid and the denser gas at elevated pressures. This leakage flow not only affects the bubble formation process but also has a great influence on other slug flow characteristics such as liquid slug length,[24] bubble velocity, which will be discussed in the following sections.

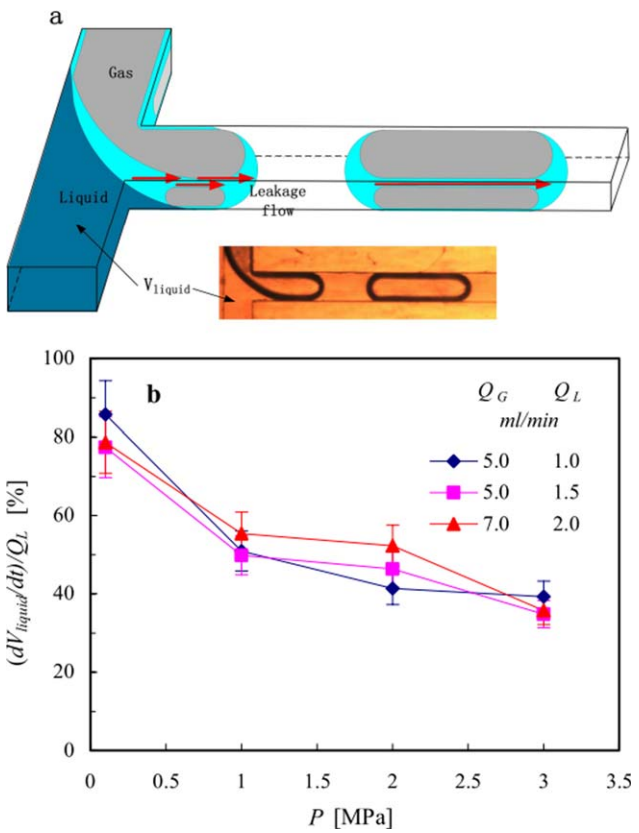

Figure 4. (a) Sketch of a bubble growing at the T-junction and the leakage flow in the channel corners around the gas bubbles and (b) estimation of the liquid flow rate from top-view images.

[Color figure can be viewed in the online issue, which is available at wileyonlinelibrary.com.]

Bubble formation dynamics

Although the formation regime has been identified, the fundamental physical mechanism, which is important in determining the size of gas bubbles, is still unclear. Many researches have been devoted to understanding the dynamic interaction between phases during the formation processes.[30,34–36] Li et al.[34] simulated the local pressure field and velocity changing periodically at the T-junction for the droplet generation using CFD. They elucidated that the surface force and viscous force alternatively dominate the droplet stream. De Menech et al.[30] monitored the pressure variance at the microchannel junction using phase field modeling for the dispersion process. It was found that the squeezing regime is characterized by an initial rise in pressure as the droplet blocks the channel width and then by a drop in pressure as the neck shrinks till pinch-off. Whereas for the shearing regime, the pressure is first increased and then kept almost stable with much smaller fluctuation. In the simulation of Ganapathy et al.,[36] similar results were obtained for the shearing regime, whereas a total different pressure variance happened in the squeezing regime. While it is convenient to use numerical methods, to monitor the pressure variance experimentally remains rather difficult, especially without interference to the original flow field. In this work, a new insight on the variation of the velocity of the forming bubble tip was presented to shed light on the gas-liquid interaction mechanism at the T-junction.

The moving velocity of the bubble tip during the formation cycle was calculated from the moving distance of the bubble tip and the time interval between adjacent frames. The results are presented in Figure 5. It can be seen that the bubble velocity is not constant and it changes periodically with the bubble formation cycle. The moving velocity of the generated gas bubble evolves at the same pace with the forming bubble tip and their values are almost identical except at the initial stages of the bubble formation. It implies that the bubble formation process has a great influence on the flow field in the main channel, which may largely enhance the mass- and heat-transfer rate.

The velocity evolution pattern under 2.0 MPa differs largely from that under 0.1 MPa as shown in Figures 5a, b. This is due to the difference in the pinch-off regime as

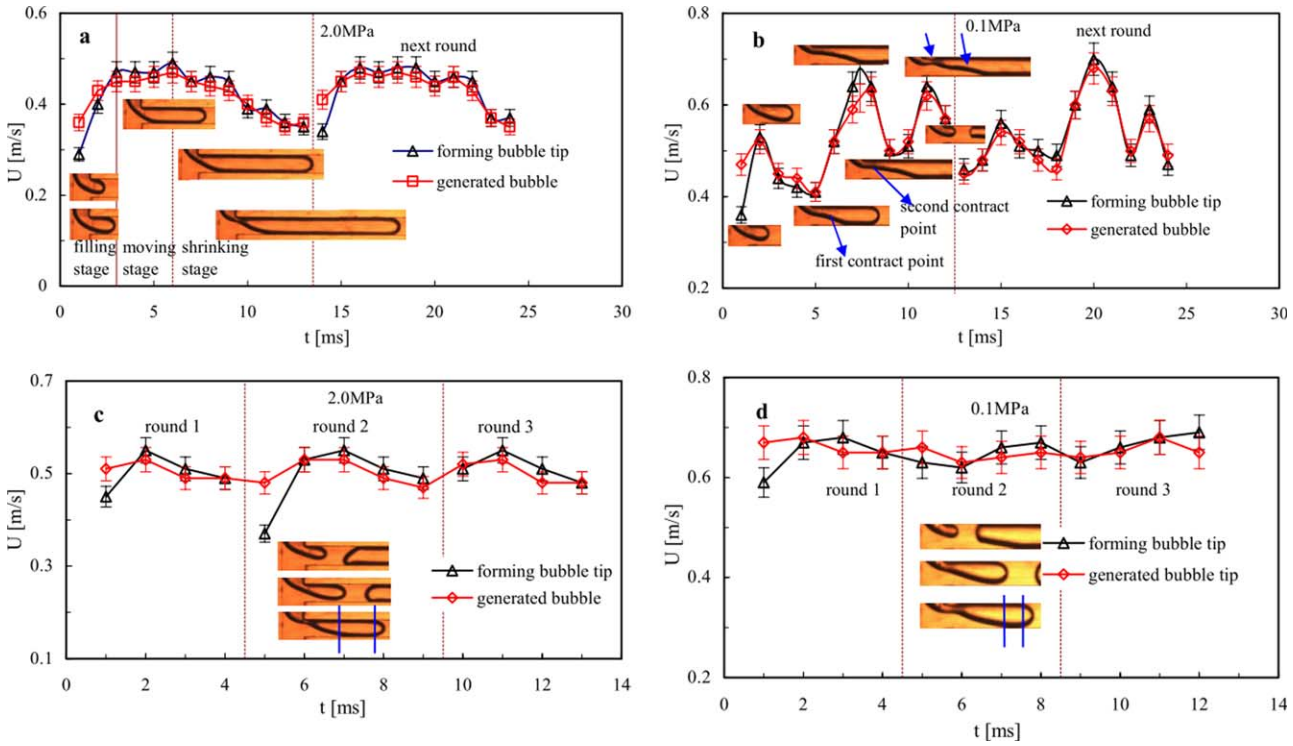

Figure 5. The evolution of the moving velocity of the generated gas bubbles and the forming bubble tips.

(a) $j_G = 0.48$ m/s, $j_L = 0.094$ m/s, $P = 2.0$ MPa; (b) $j_G = 0.48$ m/s, $j_L = 0.094$ m/s, $P = 0.1$ MPa; (c) $j_G = 0.48$ m/s, $j_L = 0.23$ m/s, $P = 2.0$ MPa; (d) $j_G = 0.48$ m/s, $j_L = 0.23$ m/s, $P = 0.1$ MPa. [Color figure can be viewed in the online issue, which is available at wileyonlinelibrary.com.]

aforementioned. In Figure 5a, the squeezing regime could be clearly categorized into three stages. The first stage is the filling stage, in which the gas tip penetrates into the liquid and moves forward until the bubble blocks the entire channel. During this stage, the bubble tip expands little and is driven by the liquid shearing force, so the velocity increases dramatically. Because the bubble tip approaches the wall opposite to the gas inlet and the moving speed is still very small, the pressure of liquid at the T-junction increases fast as well.[34,35] In the second stage, the forces on the bubble tip are temporarily balanced, so the tip just moves downstream along the main channel while the bubble neck keeps nearly constant or contracts very slowly. The bubble tip moves at a relatively high velocity with the pushing of the liquid as well as the input of the gas source. After the moving stage is the shrinking stage where the bubble neck shrinks drastically until pinch-off. During this stage, the flow resistance enlarges as the bubble keeps growing longer and so the liquid starts to squeeze the bubble neck. Due to the increased flow resistance and the occupation of the liquid in the vacated space as the bubble neck shrinks, the bubble velocity decreases. Unlike the squeezing regime shown in Figure 5a, the pattern of velocity vs. time under transition regime at atmospheric condition is much more complex as shown in Figure 5b. Both the velocities of the forming and generated bubbles fluctuate frequently and the patterns of different formation cycles may differ a lot from each other. This may be caused by the fact that the shear stress exerted on the bubble neck increases the Plateau–Rayleigh instability, which is a trigger of the gas bubble formation from a continuous thread.[33] It is noteworthy that there are two contraction points during the formation process. The first contraction happens when the bubble tip blocks the channel resulting from the squeezing of liquid, thereby leading to the appearance of a concave gas-liquid interface. Then, the forming bubble together with the contraction point is pushed down as the liquid keeps squeezing. During this stage, the bubble neck scarcely shrinks and the moving velocity increases. When the flow resistance increases with the growing of the bubble, the second contraction is triggered also by squeezing. But the shrinkage is accelerated by the shear stress and other factors such as the inertia of the forming bubble[24] and maybe a sudden back flow of liquid to the neck from the downstream thread as indicated by van steijn et al.[33] The shrinking neck detaches earlier and farther from the wall than that in squeezing regime, which is more clearly shown in Figure 3.

The evolution of the bubble velocity at a higher liquid velocity is shown in Figures 5c, d. Fluctuation in the moving velocity here is much smaller. This is because that the formation process is very fast and the bubble neck is always very narrow during the process. Hence, the perturbation of the bubble tip to the flow field is very small compared to the entire flow with high velocities. The flow in Figure 5d at 0.1 MPa is more stable than the flow in Figure 5c at 2.0 MPa, which may be explained by that the resistance originated from the bubble blockage would also contribute to the fluctuation as the blockage area of the gas bubble is larger at 2.0 MPa as shown in the figures.

Effect of pressure on bubble formation frequency

The gas bubble formation frequency was estimated by counting the number of the generated bubbles in a specified time interval (0.2 s for the majority of the experimental conditions). The effect of pressure on the frequency (f) is displayed in Figure 6. It can be seen that f decreases with an

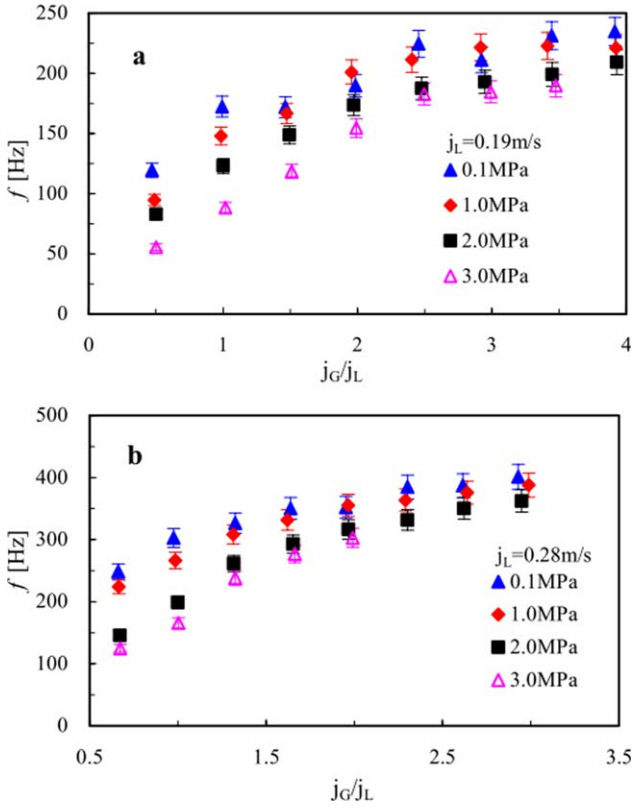

Figure 6. The effect of pressure on the bubble formation frequency.

[Color figure can be viewed in the online issue, which is available at wileyonlinelibrary.com.]

increase in the operating pressure. This is reasonable as significant amount of liquid leaks through the corner gutters as the pressure increases. Both the squeezing and shearing of liquid on the bubble neck reduce, resulting in longer formation duration under elevated pressures. Also, the increase in the density of the bubble neck makes the rupture of the gas bubble much difficult. This tendency is more obvious at small gas velocities when the inertia of the emerging bubble is smaller as shown in Figure 6a because the reduced inertia slows down the bubble rupture.[24] It can be also seen that f increases with an increase in gas superficial velocity and tends to reach an asymptotic value. This phenomenon was also observed by Arias et al.[37] and was explained by the existence of a limiting scale for bubble generation process, which is the time needed by the liquid flow to cross a distance on the order of the capillary size.

Effect of pressure on the gas bubble and liquid slug length

The effect of pressure on the lengths of the gas bubble is displayed in Figure 7. For a given liquid velocity, the gas bubble length increases linearly with the gas superficial velocity. This linear increase is in agreement with the model proposed by Garstecki et al.[26] The distinction between the bubble lengths obtained under different pressures is not obvious in spite of the relatively longer bubble formation period at higher operating pressures. It may result from the increase of the bubble cross-sectional area in the channel cross section as the system pressure increases. A set of gas bubbles under different pressures is shown in Figure 8. It can be seen from the amplified images that the dark region caused by the strong light reflection at the gas-liquid interface curvature is clearly larger while the bright area encircled by the dark region is smaller at 0.1 MPa. This means that the cross-sectional area of bubbles is smaller than that under elevated pressures because the gas is more compressible at 0.1 MPa. However, the difference between 1.0, 2.0, and 3.0 MPa can not be observed from the images. So, the 2-D images can only provide a qualitative explanation between atmospheric and elevated pressure conditions. More precise information on the bubble area and the liquid film thickness around the bubbles under different system pressures needs to be characterized with 3-D imaging technology. Based on the proposed bubble cross section model 1 and model 2 in our previous work,[24] the volume of a single bubble was calculated and the error between the two models ranges from 7.6 to 13.7%. The bubble volume would be even smaller if the gas bubble shape turns into ellipsoid as the liquid film thickness increases.[38,39] Thus, the bubble volume may deviate a lot even with the same bubble length. If the difference in the bubble frequency is comparable to the difference in the bubble surface area, the difference in the bubble length may not be obvious. However, when the effect of the increase in the formation period is dominant over the

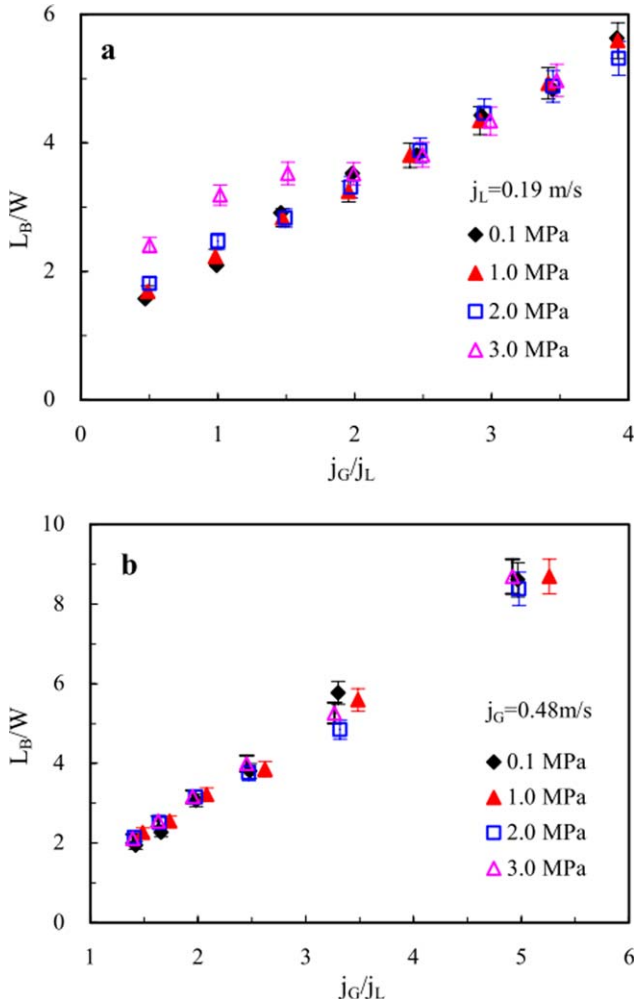

Figure 7. The effect of pressure on the gas bubble length.

[Color figure can be viewed in the online issue, which is available at wileyonlinelibrary.com.]

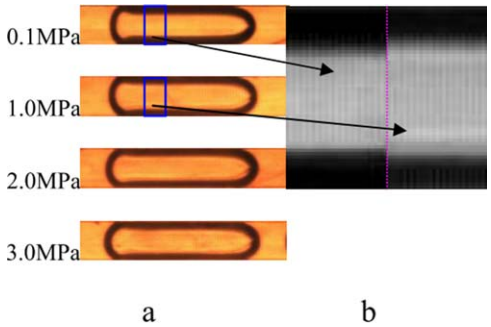

Figure 8. Increase of the bubble cross-sectional area with increasing pressure, $j_G = 0.48$ m/s, $j_L = 0.19$ m/s (a) captured images and (b) amplified grayscale images for comparison between 0.1 and 1.0 MPa.

[Color figure can be viewed in the online issue, which is available at wileyonlinelibrary.com.]

effect of the bubble cross-sectional area, the bubble length would increase obviously, as shown in Figure 7a at very small gas velocities.

Figure 9 presents the dimensionless liquid slug length as a function of j_G/j_L at different operating pressures. It can be seen that the liquid slug length decreases when either the gas or the liquid superficial velocity increases, as displayed in Figures 9a, b, respectively. To the best of our knowledge,[40–46] this kind of evolution in the liquid slug length in rectangular microchannels was first reported in our previous work.[24] The negative correlation between the liquid flow rate and the slug length was explained by the strong leakage flow around the gas bubble as described above. Völkel[45] scaled the liquid slug length linearly with the liquid flow rate by assuming that the influence of the leakage flow could be neglected in their work. The amount of the leakage flow may relate to the magnitude of the liquid flow rate, which is much higher here than that in his work. To verify this, additional experiments ($j_G = 0.004$ m/s; $j_L = 0.0093$, 0.0231, 0.0463 m/s) were conducted under 3.0 MPa. It was found that the liquid slug length increased with an increase in the liquid superficial velocity, as shown in Figure 10. Therefore, the amount of liquid in a slug would reduce even though the liquid flow rate increases as long as the leakage is large enough.

A strong influence of the system pressure on the slug length is also observed in Figure 9. The slug length decreases with an increase in the system pressure. As the leakage flow has been proven to be more pronounced under elevated pressures, it is clearly reasonable. From 0.1 to 1.0 MPa, the slug length decreases fast and the decline slows down above 1.0 MPa, indicating that the leakage flow first experiences a rapid increase and then the growth rate slows down when the system pressure is elevated, which is in accordance with the estimation in Figure 4b. However, when the flow rate is very small, the effect of the increased bubble formation time is dominant over the effect of the leakage flow. Then the tendency is reversed, as shown in Figure 9a.

As the lengths of the gas bubble and the liquid slug have a direct impact on mass transfer under slug flow in microchannels,[12,13] the prediction of these parameters are of great importance, especially under elevated pressures relevant to practical uses. Because the influence of pressure on the bubble length is not significant, only *We*, which represents the ratio of inertial to capillary forces, is taken into consideration

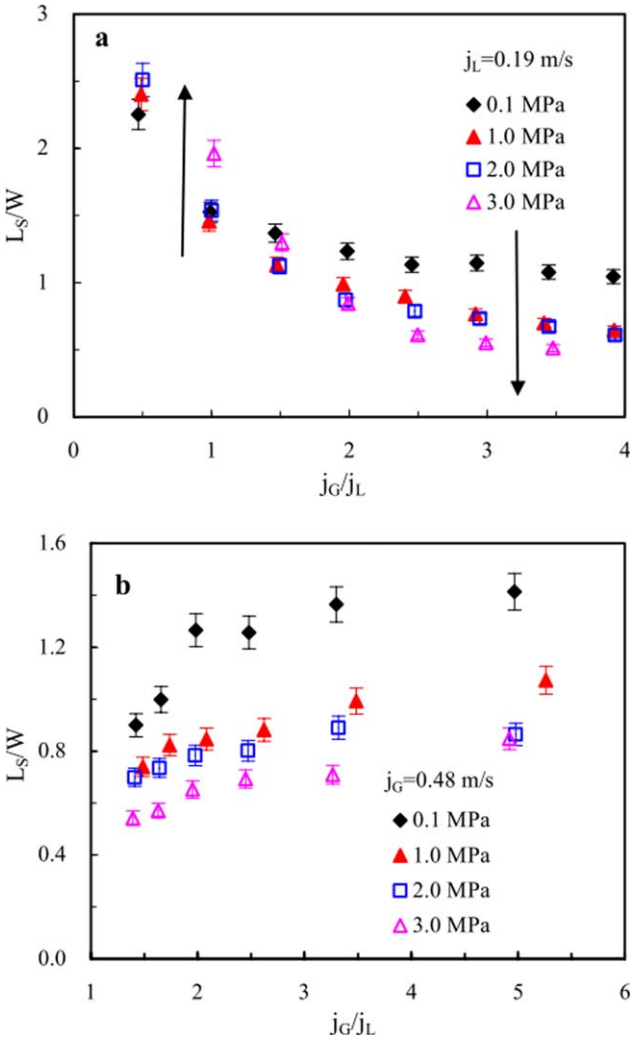

Figure 9. The effect of pressure on the liquid slug length.

[Color figure can be viewed in the online issue, which is available at wileyonlinelibrary.com.]

as a modification of the Garstecki model.[26] Regression of the experimental data provides the following correlation for the dimensionless bubble length

$$L_B/W = (1 + 1.25We^{-0.843})j_G/j_L \quad (4)$$

For the estimation of the liquid slug length under different pressures, an empirical correlation is proposed

$$L_S/W = 0.918(j_G/j_{TP})^{-0.373}(j_L/j_{TP})^{-0.373}We^{(-0.357-0.126\ln(P/P_a))} \quad (5)$$

Figure 10. The relationship between the liquid slug length and liquid superficial velocity under 3.0 MPa, (a) $j_G = 0.004$ m/s, $j_L = 0.0093$ m/s; (b) $j_G = 0.004$ m/s, $j_L = 0.0231$ m/s; and (c) $j_G = 0.004$ m/s, $j_L = 0.0463$ m/s.

[Color figure can be viewed in the online issue, which is available at wileyonlinelibrary.com.]

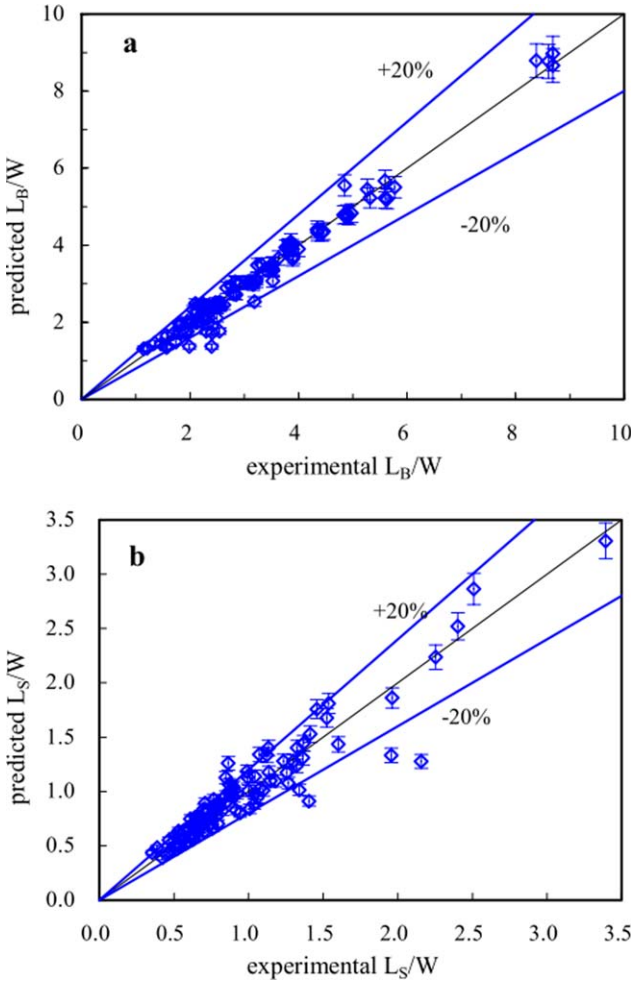

Figure 11. Predictions of (a) bubble length and (b) slug length vs. experimental values.

[Color figure can be viewed in the online issue, which is available at wileyonlinelibrary.com.]

A total of 99 sets of the experimental data were correlated for the current T-junction microchannel with parameters in the following range: $0.09 < j_G < 0.93$ m/s, $0.09 < j_L < 0.47$ m/s, $0.45 < We < 9.48$, and $0.004 < Ca < 0.016$. It can be seen in Figure 11 that both the predictions of Eqs. 4 and 5 show good agreement with the experimental results except for several data points obtained at the smallest gas velocities. The scattered points in Figure 11b may be due to the fact that *We* can only partly represent the effect of the leakage flow. Therefore, more efforts need to be taken for the study of the leakage flow.

Effect of pressure on bubble velocities

The gas bubbles under slug flow are isolated from the channel wall by a thin film region. Using the concept of macroscopically homogeneous medium, the relationship between the bubble velocity and the velocity of the liquid in the slug can be formulated according to the mass conservation law or the volume continuity.

$$U_B A_B + U_{film} A_{film} = U_S A_{mc} \tag{6}$$

For simplicity, the mean velocity of the liquid slug could be expressed as the two-phase mixture velocity, j_{TP}. The bubble velocity then is derived as

$$U_B = \frac{A_{mc}}{A_B} j_{TP} - \frac{U_{film} A_{film}}{A_B} \tag{7}$$

If the velocity of the liquid film can be neglected, the bubble velocities should be linear with j_{TP}[40,47,48] and the coefficient equals to the ratio of the cross-sectional area of the gas bubble to that of the microchannels. Yet, this only represents an averaged measurement when the film velocity or the leakage flow can not be neglected.[24] As indicated in the bubble formation section, the bubble velocity changes periodically with the bubble formation process. Therefore, all the bubble velocity data presented in this work are averaged values.

The bubble velocity is plotted vs. the two-phase mixture velocity in Figure 12. The linear relationship seems to exist at different pressures. However, the bubble velocity decreases at higher system pressures, which is also due to the increased leakage flow under high pressure and less liquid pushing the gas bubble. Interestingly, during experiments it was found that the increase rate of the bubble velocity with respect to the liquid velocity at a fixed gas superficial velocity was always smaller than that with respect to the gas velocity at a fixed liquid velocity, namely

$$\left.\frac{\Delta U_B}{\Delta j_L}\right|_{j_G} < \left.\frac{\Delta U_B}{\Delta j_G}\right|_{j_L} \tag{8}$$

The tendency was more obvious under elevated pressures, which is an additional proof for the leakage flow in the corners.

Effect of pressure on gas hold-up

The volumetric gas hold-up (ε) is an important parameter in gas-liquid two-phase flow as it is indicative of the flow regime and heat or mass transfer. The time-averaged gas hold-up was estimated from the captured images under each operating condition. The interested region is selected in a range of 300–1280 pixels for each image, which corresponds to a region about 3.3 to 14.0 mm downstream the T-junction. The bubble shape becomes regular and keeps unchanged in this region. The gas hold-up was obtained by calculating the total volume of all gas bubbles in each image based on model 1 of the cross-sectional bubble shape

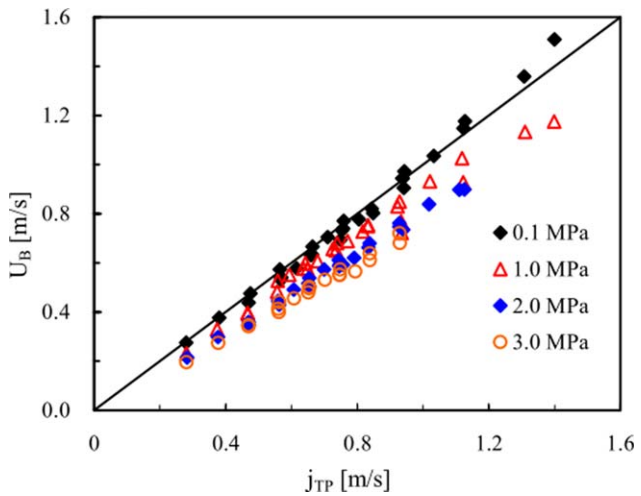

Figure 12. Bubble velocity vs. two-phase mixture velocity.

[Color figure can be viewed in the online issue, which is available at wileyonlinelibrary.com.]

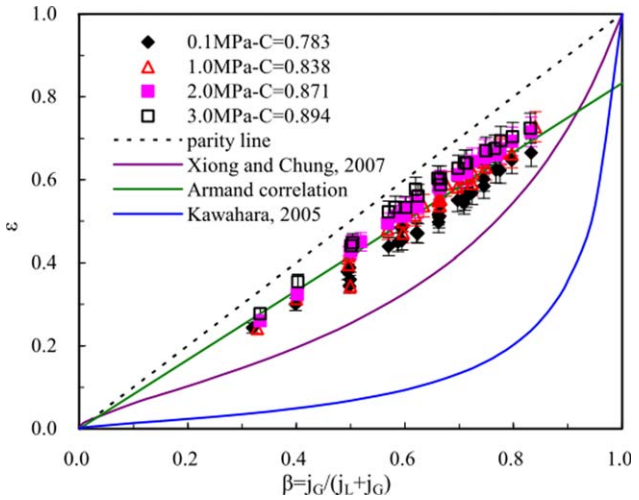

Figure 13. Gas hold-up as a function of the volumetric quality.

[Color figure can be viewed in the online issue, which is available at wileyonlinelibrary.com.]

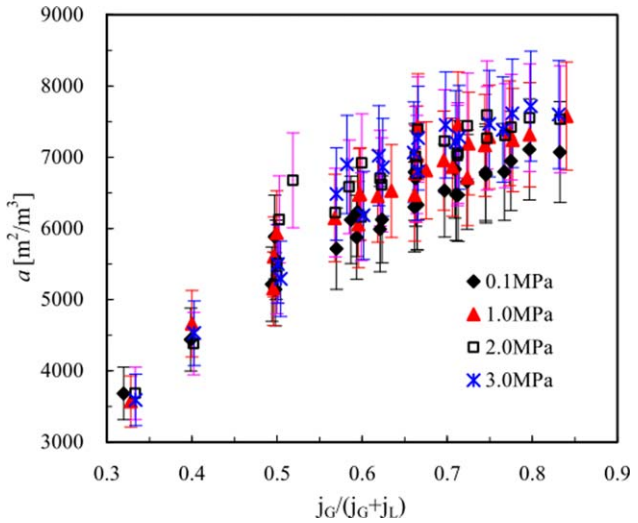

Figure 14. Specific surface area under different pressures.

[Color figure can be viewed in the online issue, which is available at wileyonlinelibrary.com.]

proposed in our previous work.[24] A comparison between the calculated gas flow rates ($Q_{cal} = f\ V_B$) and the actual mean flow rates in the microchannel showed consistency with error less than 20%. The change in the shape of the gas bubble cross-sectional area was not accounted here, but the results could also be indicative. The gas hold-up can be regarded as the homogeneous void fraction in the cross section of the channel.[49,50]

Generally, the gas hold-up correlation for microchannels as a function of the gas volumetric quality can be classified into two types[24]; linear relationship of the Armand-type $\alpha = C\beta$ and nonlinear relationship of $\alpha = C_1\beta^{0.5}/(1-C_2\beta^5)$. Which type describes well the gas hold-up is mainly dependent on the channel size.[24,50,51] Besides the channel size, there are many factors that can affect the gas hold-up such as fluid property,[51] experimental setup,[52] channel length,[53] and channel geometry.[54] This study investigated the impact of the system pressure. As shown in Figure 13, the gas hold-up in the current rectangular microchannel can be described by the Armand-type correlation as it evolves linearly with the volumetric quality of the gas phase. The effect of the system pressure is found to increase the gas hold-up at elevated pressures. Such change is obvious as the liquid slug length decreases while the gas bubble length keeps almost the same when the pressure increases. At the smallest gas velocities when the gas bubble length increases with the system pressure, the gas hold-up at elevated pressures still can be fitted by the Armand-type correlation because the liquid slug also increases. A stronger leakage flow around the bubble reduces the velocity slip ratio between the gas and the liquid, which also suggests a higher gas hold-up.

The effect of pressure on specific surface area

The specific surface area (a) is a very important parameter in multiphase mass-transfer process. Because of the uniform distribution of gas bubbles in slug flow, the determination of the specific surface area is very convenient by use of physical method. The method of calculating the surface area is similar to that for determining the gas hold-up by assuming the cross-sectional shape of the gas bubble. The results are shown in Figure 14. As can be seen, a varies from 3500 to 7700 m^2/m^3 under the experimental conditions. These values, within the range of reported data by chemical methods,[6,13] are at least one or two orders of magnitude higher than those in conventional gas-liquid contactors.[6] The specific surface area increases with an increase in the gas quality, but in a logarithm manner, which is different from that for the gas hold-up. This is because that the area of the bubble caps also contributes largely to the total surface area.

It can also be seen in Figure 14 that when the system pressure is elevated to 1.0 MPa from atmospheric pressure, the specific surface area increases a lot. However, the impact of pressure is not significant as the system pressure further increases. The larger mass-transfer area under elevated pressures implies a better mass-transfer performance, which is more attractive for gas-liquid processes such as absorption

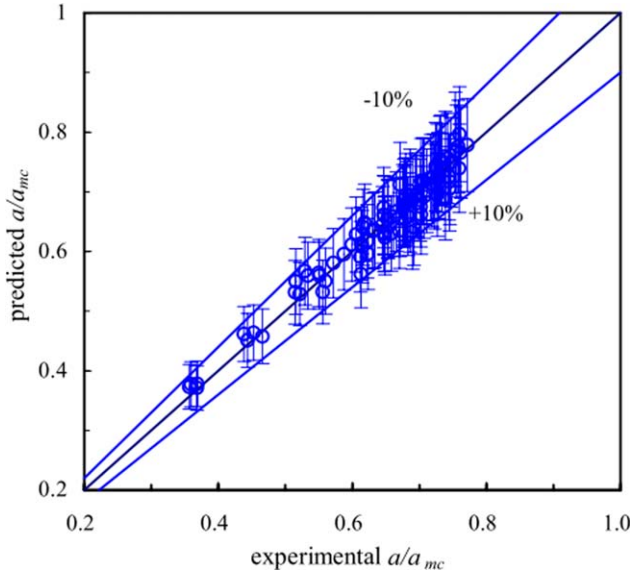

Figure 15. Prediction of dimensionless specific surface area vs. experimental values.

[Color figure can be viewed in the online issue, which is available at wileyonlinelibrary.com.]

and reaction in microchannels.[3] To interpret the specific surface area of slug flow under elevated pressures up to 3.0 MPa, an empirical correlation is developed as

$$a/a_{mc} = (0.449 - 0.086P_a/P)\ln\beta - 0.086P_a/P + 0.871 \quad (9)$$

where a_{mc} represents the specific surface area of the microchannel at 10,000 m^2/m^3. The predictions of Eq. 9 are in good agreement with the experimental results, as displayed in Figure 15. The range of validity of this equation is the same as that of Eqs. 4 and 5.

Conclusion

This study focuses on the slug flow behavior under different system pressures in a rectangular microchannel with a T-junction entrance. Visualization experiments using a high-speed camera has been carried out to study the gas bubble generation process, lengths of the gas bubble and liquid slug, bubble velocity, the gas hold-up, and the specific surface area. As gas-liquid processes in the chemical industry are commonly handled under high pressures, the findings of this work may serve as a useful guidance for the design and application of gas-liquid microreactors.

A new insight on the moving velocity of the forming bubble tip as well as that of the generated bubbles during the bubble formation process was presented, showing that the bubble velocity is not constant and varies periodically with the formation cycle. This induces a strong disturbance to the flow in the main microchannel, which may benefit the mass and heat transfer. To represent the high-throughput conditions common in the process industry, large flow rates are chosen that the *Re* varies over several hundreds. Under these conditions, the shear stress and inertial forces play important roles in the gas bubble rupture process which we claim to be in the transition regime. This study shows that the shear stress becomes less significant at elevated pressures, leading to a shift from the transition regime to the squeezing regime as the system pressure increases. This is due to a strong leakage flow around the gas bubble which increases with an increase in the system pressure. As significant amount of liquid leaks through the corner gutters, both the shear stress and the squeezing from the liquid reduce, resulting in a longer bubble formation period. However, the length of the gas bubble is kept almost unchanged as the cross-sectional bubble area increases at the same time. This leakage flow also reduces the liquid slug length and bubble velocities under high system pressures. The gas hold-up was found to vary linearly with the gas volumetric quality and increases as the pressure rises, which indicates a smaller velocity slip ratio between the gas and the liquid. The specific surface area was calculated based on a bubble model[24] and varies from 3500 to 7700 m^2/m^3 under the experimental conditions, which increases as the pressure increases.

Acknowledgments

The authors acknowledge gratefully the financial supports for this project from National Natural Science Foundation of China (Nos. 21225627, 21106141) and Ministry of Science and Technology of China (No. 2012BAA08B02).

Notation

a = specific surface area, m^2/m^3
A = cross-sectional area, m^2
Ca = capillary number defined by $(\mu_L j_{TP}/\sigma_L)$
D_H = hydraulic diameter, μm
f = bubble frequency, HZ
j = superficial velocity, m/s
P = pressure, MPa
P_a = atmospheric pressure, 0.1 MPa
Q = flow rate, mL/min
U = velocity, m/s
W = channel width
Re = two-phase Reynolds number defined by $(\rho_L u D_H/\mu_L)$, dimensionless
We = two-phase Weber number defined by $(\rho_L u^2 D_H/\sigma_L)$, dimensionless

Greek letters

β = gas volumetric quality, dimensionless
ε = gas hold-up, dimensionless

Subscripts

B = bubble
G = gas
L = liquid
S = slug
s = gas-liquid separator
mc = microchannel
TP = two phase

Literature Cited

1. Hessel V, Angeli P, Gavriilidis A, Löwe H. Gas-liquid and gas-liquid-solid microstructured reactors contacting principles and applications. *Ind Eng Chem Res*. 2005;44:9750–9769.
2. Chen GW, Yue J, Yuan Q. Gas-liquid microreaction technology: recent developments and future challenges. *Chin J Chem Eng*. 2008; 16(5):663–669.
3. Ye CB, Dang MH, Yao CQ, Chen GW, Yuan Q. Process analysis on CO_2 absorption by monoethanolamine solutions in microchannel reactors. *Chem Eng J*. 2013;225:120–127.
4. Gao NN, Wang J, Lei S, Chen JF. Removal of carbon dioxide by absorption in microporous tube-in-tube microchannel reactor. *Ind Eng Chem Res*. 2011;50(10):6369–6374.
5. Cubaud T, Sauzade M, Sun R. CO_2 dissolution in water using long serpentine microchannels. *Biomicrofluidics*. 2012;6(2):022002.
6. Yue J, Chen GW, Yuan Q, Luo LA, Gonthier Y. Hydrodynamics and mass transfer characteristics in gas–liquid flow through a rectangular microchannel. *Chem Eng Sci*. 2007;62(7):2096–2108.
7. Zhao YC, Yao CQ, Chen GW, Yuan Q. Highly efficient synthesis of cyclic carbonate with CO_2 catalyzed by ionic liquid in a microreactor. *Green Chem*. 2013;15(2):446–452.
8. Keybl J, Jensen KF. Microreactor system for high-pressure continuous flow homogeneous catalysis measurements. *Ind Eng Chem Res*. 2011;50(19):11013–11022.
9. Trachsel F, Hutter C, Rudolf von Rohr P. Transparent silicon/glass microreactor for high-pressure and high-temperature reactions. *Chem Eng J*. 2008;135:309–316.
10. Triplett KA, Ghiaasiaan SM, Abdel-Khalik SI, Sadowski DL. Gas-liquid two-phase flow in microchannels Part I: two-phase flow patterns. *Int J Multiphase Flow*. 1999;25(3):377–394.
11. Akbar MK, Plummer DA, Ghiaasiaan SM. On gas–liquid two-phase flow regimes in microchannels. *Int J Multiphase Flow*. 2003;29(5):855–865.
12. Vandu CO, Liu H, Krishna R. Mass transfer from Taylor bubbles rising in single capillaries. *Chem Eng Sci*. 2005;60(22):6430–6437.
13. Sobieszuk P, Pohorecki R, Cygański P, Grzelka J. Determination of the interfacial area and mass transfer coefficients in the Taylor gas–liquid flow in a microchannel. *Chem Eng Sci*. 2011;66(23):6048–6056.
14. Fries DM, Trachsel F, Rudolf von Rohr P. Segmented gas–liquid flow characterization in rectangular microchannels. *Int J Multiphase Flow*. 2008;34(12):1108–1118.
15. Thulasidas TC, Abraham MA, Cerro RL. Bubble-train flow in capillaries of circular and square cross-section. *Chem Eng Sci*. 1995; 50(2):183–199.
16. Günther A, Khan SA, Thalmann M, Trachsel F, Jensen KF. Transport and reaction in microscale segmented gas–liquid flow. *Lab Chip*. 2004;4:278–286.
17. Thulasidas TC, Abraham MA, Cerro RL. Flow patterns in liquid slugs during bubble-train flow inside capillaries. *Chem Eng Sci*. 1997;52(17):2947–2962.

18. Maalej S, Benadda B, Otterbein M Influence of pressure on the hydrodynamics and mass transfer parameters of an agitated bubble reactor. *Chem Eng Technol*. 2001;24:77–84.
19. Letzel HM, Schouten JC, Krishna R, van den Bleek CM. Gas holdup and mass transfer in bubble column reactors operated at elevated pressure. *Chem Eng Sci*. 1999;54:2237–2246.
20. Maalej S, Benadda B, Otterbein M. Interfacial area and volumetric mass transfer coefficient in a bubble reactor at elevated pressures. *Chem Eng Sci*. 2003;58(11):2365–2376.
21. Marre S, Adamo A, Basak S, Aymonier C, Jensen KF. Design and packaging of microreactors for high pressure and high temperature applications. *Ind Eng Chem Res*. 2010;49(22):11310–11320.
22. Verboom W. Selected examples of high-pressure reactions in glass microreactors. *Chem Eng Technol*. 2009;32(11):1695–1701.
23. Zhao YC, Chen GW, Ye CB, Yuan Q. Gas–liquid two-phase flow in microchannel at elevated pressure. *Chem Eng Sci*. 2013;87:122–132.
24. Yao CQ, Zhao YC, Ye CB, Dang MH, Dong ZY, Chen GW. Characteristics of slug flow with inertial effects in a rectangular microchannel. *Chem Eng Sci*. 2013;95:246–256.
25. Baranenko VI, Sysoev VS, Fałkovskii LN, Kirov VS, Piontkovskii AI, Musienko AN. The solubility of nitrogen in water. *Sov At Energy*. 1990;68(2):162–165.
26. Garstecki P, Fuerstman MJ, Stone HA, Whitesides GM. Formation of droplets and bubbles in a microfluidic T-junction-scaling and mechanism of break-up. *Lab Chip*. 2006;6(3):437–446.
27. van Steijn V, Kleijn CR, Kreutzer MT. Predictive model for the size of bubbles and droplets created in microfluidic T-junctions. *Lab Chip*. 2010;10(19):2513–2518.
28. Guo F, Chen B. Numerical study on Taylor bubble formation in a micro-channel T-junction using VOF method. *Microgravity Sci Technol*. 2009;21(S1):51–58.
29. Yue J, Luo LA, Gonthier Y, Chen GW, Yuan Q. An experimental investigation of gas–liquid two-phase flow in single microchannel contactors. *Chem Eng Sci*. 2008;63(16):4189–4202.
30. de Menech M, Garstecki P, Jousse F, Stone HA. Transition from squeezing to dripping in a microfluidic T-shaped junction. *J Fluid Mech*. 2008;595:141–161.
31. Wong H, Radke CJ, Morris S. The motion of long bubbles in polygonal capillaries. Part 2. Drag, fluid pressure and fluid flow. *J Fluid Mech*. 1995;292:95–100.
32. van Steijn V, Kreutzer MT, Kleijn CR. μ-PIV study of the formation of segmented flow in microfluidic T-junctions. *Chem Eng Sci*. 2007;62(24):7505–7514.
33. van Steijn V, Kleijn CR, Kreutzer MT. Flows around confined bubbles and their importance in triggering pinch-off. *Phys Rev Lett*. 2009;103(21):214501.
34. Li XB, Li FC, Yang JC, Kinoshita H, Oishi M, Oshima M. Study on the mechanism of droplet formation in T-junction microchannel. *Chem Eng Sci*. 2012;69(1):340–351.
35. Yan Y, Guo D, Wen SZ. Numerical simulation of junction point pressure during droplet formation in a microfluidic T-junction. *Chem Eng Sci*. 2012;84:591–601.
36. Ganapathy H, Al-Hajri E, Ohadi MM. Phase field modeling of Taylor flow in mini/microchannels, Part I: bubble formation mechanisms and phase field parameters. *Chem Eng Sci*. 2013;94:138–149.
37. Arias S, Ruiz X, Casademunt J, Ramírez-Piscina L, González-Cinca R. Experimental study of a microchannel bubble injector for microgravity applications. *Microgravity Sci Technol*. 2009;21(1–2):107–111.
38. Hazel AL, Heil M. The steady propagation of a semi-infinite bubble into a tube of elliptical or rectangular cross-section. *J Fluid Mech*. 2002;470:91–114.
39. Kuzmin A, Januszewski M, Eskin D, Mostowfi F, Derksen JJ. Three-dimensional binary-liquid lattice Boltzmann simulation of microchannels with rectangular cross sections. *Chem Eng J*. 2011;178:306–316.
40. Abadie T, Aubin J, Legendre D, Xuereb C. Hydrodynamics of gas–liquid Taylor flow in rectangular microchannels. *Microfluid Nanofluidics*. 2012;12(1–4):355–369.
41. Liu H, Vandu CO, Krishna R. Hydrodynamics of Taylor flow in vertical capillaries: flow regimes, bubble rise velocity, liquid slug length, and pressure drop. *Ind Eng Chem Res*. 2005;44:4884–4897.
42. Laborie S, Cabassud C, Durand-Bourlier L, Lainé JM. Characterisation of gas-liquid two-phase flow inside capillaries. *Chem Eng Sci*. 1999;54(23):5723–5735.
43. Leclerc A, Philippe R, Houzelot V, Schweich D, de Bellefon C. Gas–liquid Taylor flow in square micro-channels: new inlet geometries and interfacial area tuning. *Chem Eng J*. 2010;165(1):290–300.
44. Qian D, Lawal A. Numerical study on gas and liquid slugs for Taylor flow in a T-junction microchannel. *Chem Eng Sci*. 2006;61(23):7609–7625.
45. Völkel N. Design and characterization of gas-liquid microreactors, PhD Thesis. France: Institut of National Polytechnique de Toulouse, 2009.
46. Pohorecki R, Kula K. A simple mechanism of bubble and slug formation in Taylor flow in microchannels. *Chem Eng Res Des*. 2008;86(9):997–1001.
47. Yue J, Luo LA, Gonthier Y, Chen GW, Yuan Q. An experimental study of air–water Taylor flow and mass transfer inside square microchannels. *Chem Eng Sci*. 2009;64(16):3697–3708.
48. Choi CW, Yu DI, Kim MH. Adiabatic two-phase flow in rectangular microchannels with different aspect ratios: part II—bubble behaviors and pressure drop in single bubble. *Int J Heat Mass Transfer*. 2010;53(23–24):5242–5249.
49. Chung PMY, Kawaji M. The effect of channel diameter on adiabatic two-phase flow characteristics in microchannels. *Int J Multiphase Flow*. 2004;30(7–8):735–761.
50. Xiong R, Chung JN. An experimental study of the size effect on adiabatic gas-liquid two-phase flow patterns and void fraction in microchannels. *Phys Fluids*. 2007;19(3):033301.
51. Kawahara A, Sadatomi M, Okayama K, Kawaji M, Chung PMY. Effects of channel diameter and liquid properties on void fraction in adiabatic two-phase flow through microchannels. *Heat Transfer Eng*. 2005;26(3):13–19.
52. Ide H, Kimura R, Kawaji M. Optical measurement of void fraction and bubble size distributions in a microchannel. *Heat Transfer Eng*. 2007;28(8–9):713–719.
53. Ide H, Kimura R, Hashiguchi H, Kawaji M. Effect of channel length on the gas–liquid two-phase flow phenomena in a microchannel. *Heat Transfer Eng*. 2012;33(3):225–233.
54. Choi CW, Yu DI, Kim MH. Adiabatic two-phase flow in rectangular microchannels with different aspect ratios: part I—flow pattern, pressure drop and void fraction. *Int J Heat Mass Transfer*. 2011;54(1–3):616–624.

Manuscript received July 16, 2013, and revision received Nov. 9, 2013.